Energy Conversion and Management 50 (2009) 69–75

Contents lists available at ScienceDirect

Energy Conversion and Management

journal homepage: www.elsevier.com/locate/enconman

Numerical investigation of coupled heat and mass transfer during desorption of hydrogen in metal hydride beds

P. Muthukumar *, A. Satheesh, U. Madhavakrishna, Anupam Dewan

Department of Mechanical Engineering, Indian Institute of Technology Guwahati, Guwahati 781039, Assam, India

ARTICLE INFO

Article history:
Received 22 January 2008
Accepted 26 August 2008
Available online 8 October 2008

Keywords:
Hydrogen storage
Desorption
Coupled heat and mass transfer
FLUENT 6.1.22

ABSTRACT

This paper presents a numerical investigation of two-dimensional coupled heat and mass transfer processes in $MmNi_{4.6}Fe_{0.4}$ and $MmNi_{4.6}Al_{0.4}$ based metal hydride beds of cylindrical configuration during desorption of hydrogen using a commercial software FLUENT 6.1.22. Temperature and concentration profiles at different radial locations, variation of average bed temperature and amount of hydrogen desorbed are presented at different hot fluid temperatures and bed thicknesses ranging from 30 to 50 °C and 5 to 15 mm, respectively. The numerical results show that the dehydriding process for both the alloys depends on the temperature distribution in the metal hydride bed. At a given hot fluid temperature of 50 °C, $MmNi_{4.6}Fe_{0.4}$ and $MmNi_{4.6}Al_{0.4}$ desorb the maximum hydrogen of about 1.11 and 1.28 wt%, respectively at the supply conditions of 30 bar and 25 °C. The present computational results are also compared with the experimental data reported in the literature and a good agreement was found between the two.
© 2008 Elsevier Ltd. All rights reserved.

1. Introduction

Use of hydrogen as a fuel in many practical applications is limited due to the problems associated with storage and transport. Recently, metal hydride based hydrogen storage systems have drawn attention over the conventional methods due to their high volumetric storage capacity, utilization of low-grade thermal inputs, compact in construction, absence of moving parts and high safety. Further it also delivers pure hydrogen irrespective of the input quality of hydrogen. The performances (defined as rates of absorption and desorption) of such system depend on the rate at which the amount of heat is supplied to, or removed from the metal hydride bed. Heat and mass transfer in metal hydride bed is a complex phenomenon where all modes of heat transfer are encountered.

Many investigators have studied the coupled heat and mass transfer characteristics of hydride bed during the absorption of hydrogen using one-dimensional mathematical model in dimensionless form without considering the effects of convection and radiation [1], using two-dimensional mathematical model without considering the effects of heat transport by convection and radiation [2], using two-dimensional mathematical model considering the convection effect and without considering the radiation effect [3–8]. Very few coupled heat and mass transfer studies in hydride beds during desorption of hydrogen are reported in the literature [9–14]. Using one-dimensional mathematical model in rectangular coordinates, Gopal and Murthy [9] studied the effects of operating parameters such as supply and delivery pressures, and hot fluid temperature on the dehydriding process without considering the effects of convection and radiation. Jemni and Nasrallah [10] predicted the dynamic behavior of heat and mass transfer in a metal hydride reaction bed during desorption of hydrogen using two-dimensional mathematical model considering the effects of convection and variation of gas pressure inside the reactor. Later, Jemni and his coworkers [11] performed an experimental investigation to determine the equilibrium pressure, reaction kinetics and thermal conductivity of $LaNi_5$–H_2 hydride bed during both absorption and desorption processes. They predicted the temperature and pressure evolutions in the reactor using theoretical model and compared these with experimental results. Their numerical results showed good agreement with the experimental data reported by them.

Askri et al. [12] developed a two-dimensional mathematical model to describe the transient heat and mass transfer during desorption of hydrogen in a porous lanthanum misch metal bed of cylindrical configuration. Subsequently, the same research group [13] investigated the dynamic behavior of heat and mass transfer during both absorption and desorption processes in $LaNi_5$ and Mg based metal hydride reaction beds using two-dimensional mathematical model considering the effects of convection and radiation. It is observed that the effect of radiative heat transfer is significant for Mg based alloys while for $LaNi_5$ alloy it is negligible. Isselhorst [14] numerically studied heat and mass transfer in $LmNi_{4.85}Sn_{0.15}$ and $LmNi_{4.49}CO_{0.1}Mn_{0.21}Al_{0.21}$. They studied the transient behavior of couple heat and mass transfer characteristics

* Corresponding author. Tel.: +91 361 2582673; fax: +91 361 2690762.
E-mail address: pmkumar@iitg.ernet.in (P. Muthukumar).

0196-8904/$ - see front matter © 2008 Elsevier Ltd. All rights reserved.
doi:10.1016/j.enconman.2008.08.028

Nomenclature

C_p	heat capacity [J/kg K]
E_d	activation energy of the reaction [J/mol H_2]
K	coefficient of Darcy law [m^2]
M_{H2}	molar mass of hydrogen [kg/kmol]
P	pressure [bar]
r	radius of the reactor [m]
R_u	ideal gas constant [J/mol K]
t	time [s]
T	temperature [K]
V	velocity [m/s]
x	fraction of desorbed hydrogen
z	length of reactor [m]
ρ	density [kg/m^3]
ϵ	porosity
λ	thermal conductivity [W/m K]
μ	dynamic viscosity [kg/m s]
σ	reaction rate constant [s^{-1}]
ΔH	enthalpy of desorption [J/mol H_2]
ΔS	entropy of desorption [J/mol H_2 K]
$\Delta\rho$	fictitious increase of the hydride density at saturation [kg/m^3]
φ_s	slope factor
φ_0	constant
φ	hysteresis factor

Subscripts

c	cold
d	desorption
e	effective
eq	equilibrium
f	final, fluid
g	gas
h	hot
i	inner
m	metal
mag	magnitude
ref	reference
s	supply
0	initial

such as hydride bed temperature, concentration, pressure distribution and the amount of hydrogen absorbed/desorbed in a metal hydride bed at differential radial and axial positions. His numerical results also showed good agreement with the experimental data reported by them.

Most of the mathematical models reported on desorption studies in literature are alloy dependent [9–14] and do not consider the effects of plateau slope and hysteresis of PCT [9]. It is also observed from the literature that most of the reported desorption studies are concentrated on the evaluation of temperature and concentration profiles and do not reveal the effects of parameters such as desorption temperature and bed thickness on the desorption characteristics of the alloy [10–14]. Further, it is evident from the literature that writing a computer program to numerically solve such a complex coupled heat and mass transfer problem by considering the effects of convection, geometrical configuration of the hydride bed, plateau slope and hysteresis of PCT etc., is tedious and also consumes tremendous time. Recently, Phate et al. [7] and Marty et al. [8] attempted to solve such coupled heat and mass transfer in hydride bed during absorption of hydrogen in cylindrical coordinates using commercial software FLUENT 6.2. However their models are alloy dependent and do not include the effects of plateau slope and hysteresis of the PCT of hydriding alloy. In a recent study, Muthukumar et al. [15] reported the numerical investigation of coupled heat and mass transfer during absorption of hydrogen in $MmNi_{4.6}Al_{0.4}$ at different operating and bed related parameters using FLUENT 6.1.22. They considered the effects of plateau slope and hysteresis of the PCT of hydriding alloy. In the present paper, the authors have extended the model of Muthukumar et al. [15] for desorption of hydrogen in $MmNi_{4.6}Fe_{0.4}$ and $MmNi_{4.6}Al_{0.4}$ at different hot fluid temperatures and reactor bed thicknesses using FLUENT 6.1.22.

2. Mathematical model

The mathematical model for the co-axial cylindrical reactor (shown in Fig. 1) considered in the present work is similar to that used by Muthukumar et al. [15,16]. $MmNi_{4.6}Fe_{0.4}$ or $MmNi_{4.6}Al_{0.4}$ hydride alloy is filled in the space between the inner reaction tube and the filter with a uniform void fraction of 0.5. The heat transfer fluid flows spirally in the space between the inner and outer concentric tubes. Since, the desorption mechanism is assumed to be axisymmetric, only half of the reactor is modeled. The computations are performed using the commercial software FLUENT 6.1.22.

The phenomena that occurs during the desorption of hydrogen is as follows

- At the start of the desorption process (time $t = 0$), the alloy is fully hydrided with hydrogen and is set at an initial temperature.
- Once the desorption is initiated, dehydrogenation takes place from the reactor and hydrogen flows through the porous metallic medium. Owing to the endothermic character of the desorption process, the bed experiences a sudden fall in temperature everywhere.
- The equilibrium pressure (P_{eq}) of the metal hydride also decreases due to a decrease of the bed temperature in accordance with the Van't Hoff equation

$$P_{eq} = \exp\left[\frac{\Delta S}{R_u} - \frac{\Delta H}{R_u T} + (\varphi_s - \varphi_0)\tan\left(\pi\left(\frac{x}{x_f} - \frac{1}{2}\right)\right) - \frac{\varphi}{2}\right] \times 10^5 \text{ N/m}^2. \quad (2.1)$$

2.1. Problem formulation

The governing equations are solved with a fully implicit finite volume numerical scheme embodied in a general purpose code FLUENT 6.1.22. The solution method involves the integration of the governing differential equations over finite control volume and transforming them into a general algebraic form. A transport equation in the general form may be written as

$$\frac{\partial(\rho\phi)}{\partial t} + \nabla\cdot(\rho u\phi) = \nabla\cdot(\Gamma\nabla\phi) + S_h, \quad (2.2)$$

where ϕ denotes a generic variable and refers to the variable being considered (i.e., u, v, T), Γ denotes the exchange coefficient and S_h the source term. This linearalized equation is solved by using the SIMPLE algorithm [17].

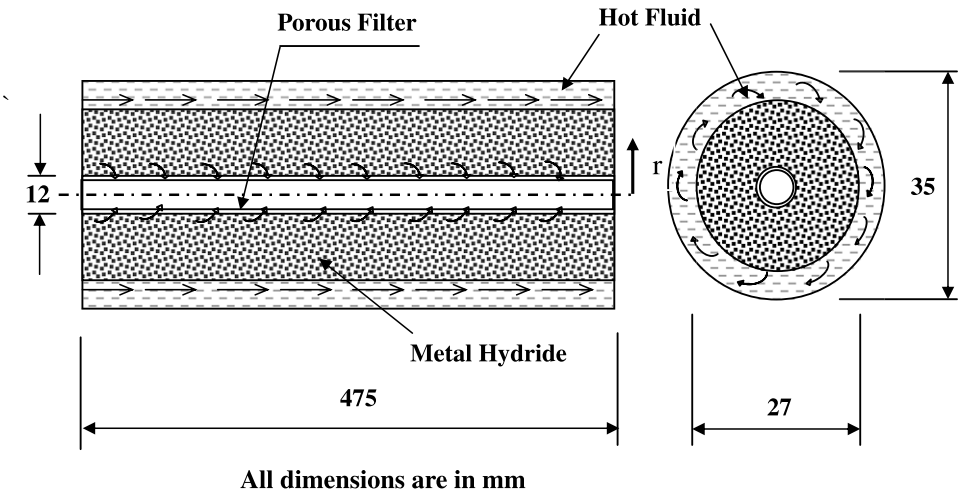


Fig. 1. Schematic of co-axial cylindrical reactor.

The assumptions made during absorption process also hold good for the desorption process.

- The gas phase is ideal from the thermodynamic viewpoint.
- The local thermal equilibrium is valid and the radiative heat transfer is negligible (this assumption is valid for all Mm, Zr and Ti based alloys whose desorption temperatures at the atmospheric pressure are well below 50 °C).

The rate of reaction is a function of the bed temperature, hydrogen pressure and hydrogen concentration in the hydride bed. The expression for the reaction kinetics is given by [9]

$$\frac{\partial x}{\partial t} = -\sigma \frac{(P_d - P_{eq})}{P_{eq}} \frac{(x - x_f)}{(x_0 - x_f)} \exp\left(\frac{-E_d}{R_u T}\right), \tag{2.3}$$

where x denotes the dehydrogenation fraction defined as the quantity obtained by dividing the mass of hydrogen desorbed to the mass desorbed at the saturation and E_d denotes the activation energy. Initially, the rate of hydrogen desorption increases rapidly and becomes zero at the end of the desorption process. This is due to a decrease of the pressure difference between equilibrium pressure (P_{eq}) and desorption pressure (P_d).

The continuity equation includes a sink term to take the amount of hydrogen desorption into account and the resulting equation per unit volume (kg/m^3 s) is given by [8]

$$\varepsilon \frac{\partial \rho_g}{\partial t} + \nabla \cdot (\rho_g \vec{V}) = \Delta\rho(1 - \varepsilon) \frac{dx}{dt}, \tag{2.4}$$

where, the gas density ρ_g is deduced from the perfect gas model

$$\rho_g = \frac{P M_{H_2}}{R_u T}. \tag{2.5}$$

The momentum equations are then solved in the porous medium using the classical Darcy law

$$\vec{\nabla} P = -\frac{\mu}{K} \vec{V}, \tag{2.6}$$

where, the coefficient K denotes permeability and is a function of the particle size of the metal hydride powder. The energy equation is given by [8]

$$(\rho C_p)_e \frac{\partial T}{\partial t} + (\rho C_p)_g \vec{V} \cdot \vec{\nabla} T = \lambda_e \nabla^2 T + \frac{\Delta\rho(1 - \varepsilon)\Delta H}{M_{H_2}} \frac{dx}{dt}, \tag{2.7}$$

where

$$(\rho C_p)_e = \varepsilon(\rho C_p)_g + (1 - \varepsilon)(\rho C_p)_m \tag{2.8}$$

and

$$\lambda_e = \varepsilon\lambda_g + (1 - \varepsilon)\lambda_m. \tag{2.9}$$

The source term on the extreme right hand side of Eq. (2.7) represents the amount of heat absorbed during the desorption process (W/m^3).

2.2. Initial and boundary conditions

Initially, at time $t = 0$ the pressure, temperature and density are assumed to be constant within the reactor

$$\rho_m(z, r) = \rho_0; \quad T_m(z, r) = T_g(z, r) = T_0; \quad P_g(z, r) = P_0. \tag{2.10}$$

The sidewalls of the reactor are subjected to the adiabatic condition and the outer periphery is subjected to uniform convective boundary condition throughout the reactor.

Along the top surface (Fig. 1) the convective boundary condition gives

$$-\lambda_e \frac{\partial T}{\partial r}(z, r)_{r=R} = U(T - T_f). \tag{2.11}$$

Along the filter section ($r = r_i$) the adiabatic condition leads to

$$\frac{\partial P_g}{\partial r}(z, r)_{r=r_i} = 0; \quad \frac{\partial T}{\partial r}(z, r)_{r=r_i} = 0. \tag{2.12}$$

Along the left face ($z = 0$) the adiabatic condition leads to

$$\frac{\partial P_g}{\partial z}(z, r)_{z=0} = 0; \quad \frac{\partial T}{\partial z}(z, r)_{z=0} = 0. \tag{2.13}$$

Along the right face (where $z = Z$) the adiabatic condition leads to

$$\frac{\partial P_g}{\partial z}(z, r)_{z=Z} = 0; \quad \frac{\partial T}{\partial z}(z, r)_{z=Z} = 0. \tag{2.14}$$

2.3. Modeling of porous region

Porous media are modeled by the addition of a momentum source term to the standard fluid flow equations. The source term consists of two parts: one is a viscous loss term and the other is the inertial loss term (the first and second terms on the right hand side of Eq. (2.15))

$$S_i = -\left(\frac{\mu}{K} v_i + C_2 \frac{1}{2} \rho v_{mag} v_i\right), \tag{2.15}$$

where S_i is the source term for the ith (x, y and z) momentum equation of porous media. K denotes the permeability and C_2 the inertial

resistance factor. Since the flow through porous media is assumed to be laminar, the pressure drop is typically proportional to velocity and it is considered as zero. Ignoring convective acceleration and diffusion, the porous media model reduces to the Darcy law.

The effective thermal conductivity in the porous medium is computed by FLUENT 6.1.22 as the volume average of the fluid conductivity and the solid conductivity. For the transient porous media calculations, the effect of porosity on the time derivative terms is accounted for all scalar transport equations and continuity equation. When the effect of the porosity is taken into account, the time derivative term becomes $\frac{\partial}{\partial t}(\varepsilon\rho\phi)$, where ϕ denotes the scalar quantity.

2.4. Method of solution

The energy equation employed in FLUENT 6.1.22 has the following form

$$\frac{\partial}{\partial t}(\rho h) + \nabla \cdot (\vec{v}\rho h) = \nabla \cdot (\lambda \nabla T) + S_h, \tag{2.16}$$

where h = sensible enthalpy = $\int_{T_{ref}}^{T} C_p dT$ and S_h = volumetric heat source.

The volumetric heat source term is enabled by incorporating a user defined function to FLUENT 6.1.22 in the same way the equilibrium pressure and the rate of reaction equations are enabled.

3. Results and discussion

A 20 × 200 grid system is employed based on the grid refinement test [15]. Table 1 shows the dimensions of the reactor, thermo-physical properties of metal hydrides, properties of hydrogen and constants used in the analysis [15,16]. The results obtained for $MmNi_{4.6}Fe_{0.4}$ and $MmNi_{4.6}Al_{0.4}$ hydride beds during the desorption process are presented at different hot fluid temperatures varying from 30 to 50 °C and the reactor bed thickness varying from 5 to 15 mm. Desorption pressure is set equal to 1.0 bar for all the cases.

Table 1
Details of reaction bed geometry, thermo-physical properties of the alloys and constants used in the model

Reactor geometry		
Length of the cylinder (mm)	475	
Inner radius of inner cylinder (mm)	4.5	
Inner radius of outer cylinder (mm)	12	
Thickness of cylinder wall (mm)	3	
Properties	$MmNi_{4.6}Al_{0.4}$	$MmNi_{4.6}Fe_{0.4}$
Density of metal (kg/m^3)	8400	8500
Specific heat of metal (J/kg K)	419	419
Effective thermal conductivity of metal (including copper additive) (W/m K)	1.6	1.6
Porosity	0.5	0.5
Effective density of solid (kg/m^3)	4200	4250
Activation energy (J/mol H_2)	21170	25000
Enthalpy formation (J/mol H_2)	28000	27500
Entropy formation (J/mol H_2 K)	107.2	105
Reaction constant (σ)	100	475
Properties of hydrogen		
Thermal conductivity of hydrogen(W/m K)	0.1272	
Specific heat of hydrogen (J/kg K)	14283	
Density of hydrogen (kg/m^3)	0.0838	
Constants		
Universal gas constant (J/mol K)	8.314	
Slope factor(φ_s)	0.35	
Constant (φ_0)	0.15	
Hystersis Factor (φ)	0.2	

3.1. Validation of numerical results

Figs. 2 and 3 show that the predicted average bed temperature profiles of $MmNi_{4.6}Fe_{0.4}$ and $MmNi_{4.6}Al_{0.4}$ based hydride beds at different hot fluid temperatures ranging from 30 to 50 °C match closely with the experimental data reported by Muthukumar et al. [16]. Due to the poor thermal conductivity of the metal hydride, the necessary amount of heat is not transferred to the metal hydride bed. Hence, the hydride bed takes the heat from the bed itself and starts to desorb the hydrogen. Due to this the temperature of the bed decreases rapidly in the initial stage up to −4 °C within 20 s for $MmNi_{4.6}Fe_{0.4}$ alloy and up to 1 °C within 10 s for $MmNi_{4.6}Al_{0.4}$ alloy. As the time progress, the temperature of the hydride bed reaches the hot fluid temperature. It is observed that the average bed temperature quickly attains the hot fluid temperature for 50 °C. At higher hot fluid temperatures, the temperature

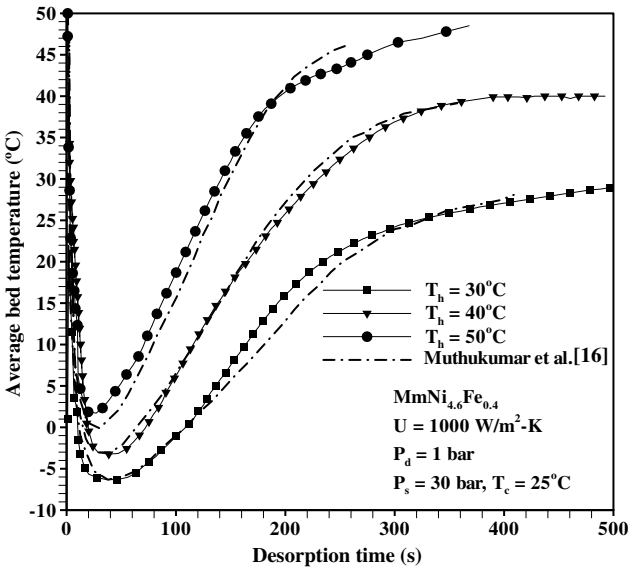


Fig. 2. Validation of the predicted average bed temperature at different hot fluid temperatures for $MmNi_{4.6}Fe_{0.4}$.

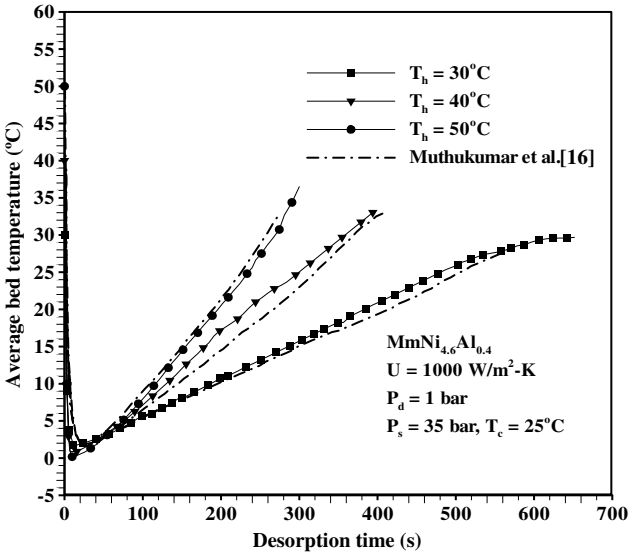


Fig. 3. Validation of the predicted average bed temperature at different hot fluid temperatures for $MmNi_{4.6}Al_{0.4}$.

differences are found to be high resulting in rapid heat transfer. Hence, due to large temperature and also the prevailing large pressure difference between hydride equilibrium pressure and desorption pressure, the dehydriding reaction is found to be rapid for temperatures higher than 40 °C. Further, due to large plateau slope of PCT, higher hot fluid temperatures also help in desorbing large amount of hydrogen.

Figs. 4 and 5 show the validation of the computed amount of hydrogen desorbed for both the alloys. $MmNi_{4.6}Fe_{0.4}$ and $MmNi_{4.6}Al_{0.4}$ desorb about 1.11 and 1.28 wt% at the supply conditions of 30 bar and 25 °C. The computations show a small deviation from the experimental data at the beginning of the process. This may be due to the assumption of larger void fraction (while in the experiments copper matrix was used in place of the void space for the improvement of the effective thermal conductivity of the hydride bed) and also due to the error in assuming the value of reaction rate constant (σ). For a given hot fluid temperature of 40 °C, $MmNi_{4.6}Fe_{0.4}$ takes about 210 s to desorb the maximum amount of hydrogen of 1.11 wt%, while $MmNi_{4.6}Al_{0.4}$ takes about 350 s to desorb about 1.28 wt%. This is mainly due to the large pressure difference between the hydrogen equilibrium and desorption pressures of the former alloy. It is expected from the numerical results that $MmNi_{4.6}Fe_{0.4}$ and $MmNi_{4.6}Al_{0.4}$ desorb the maximum amounts of hydrogen of 1.6 and 1.3 wt%, respectively, when they are subjected to the supply conductions of 35 bar supply pressure and 15 °C absorption temperature [16]. Further, it is also observed from Figs. 4 and 5 that the higher hot fluid temperatures (above 40 °C) reduce the desorption time significantly.

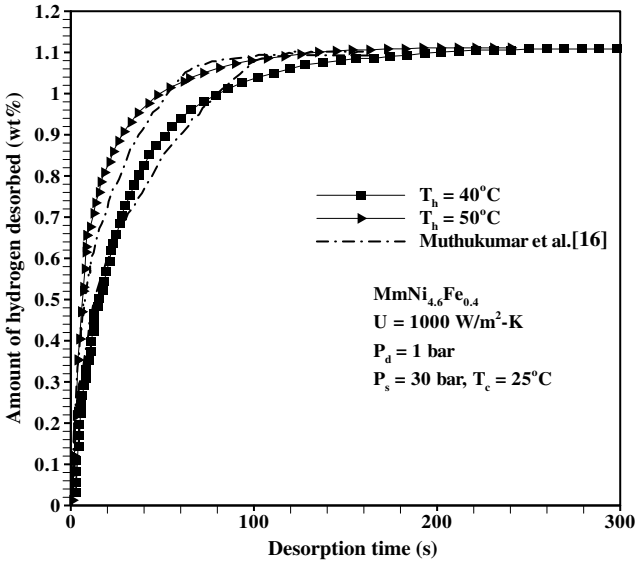


Fig. 4. Validation of the predicted amount of hydrogen desorbed at different hot fluid temperatures for $MmNi_{4.6}Fe_{0.4}$.

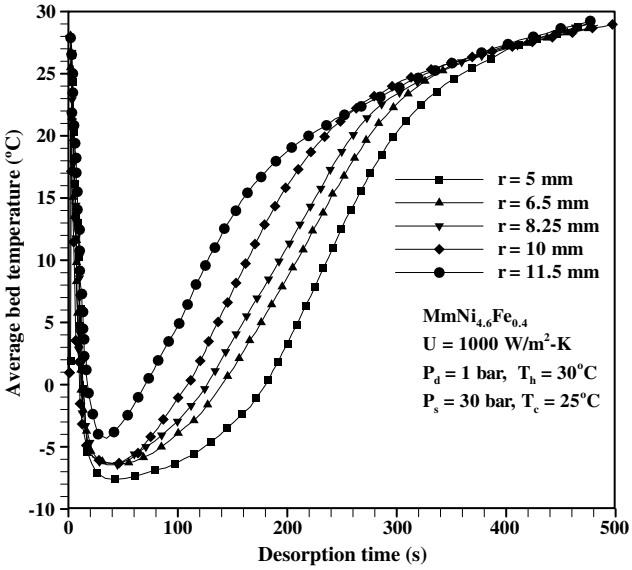


Fig. 6. Variation of average bed temperature at different radial positions for$MmNi_{4.6}Fe_{0.4}$.

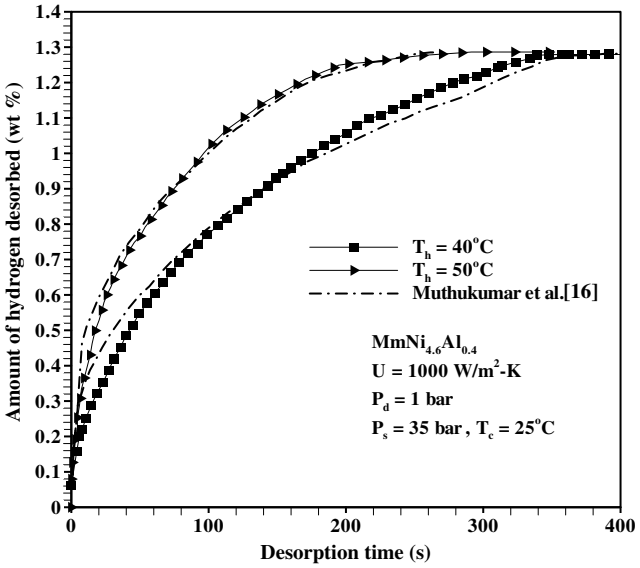


Fig. 5. Validation of the predicted amount of hydrogen desorbed at different hot fluid temperatures for $MmNi_{4.6}Al_{0.4}$.

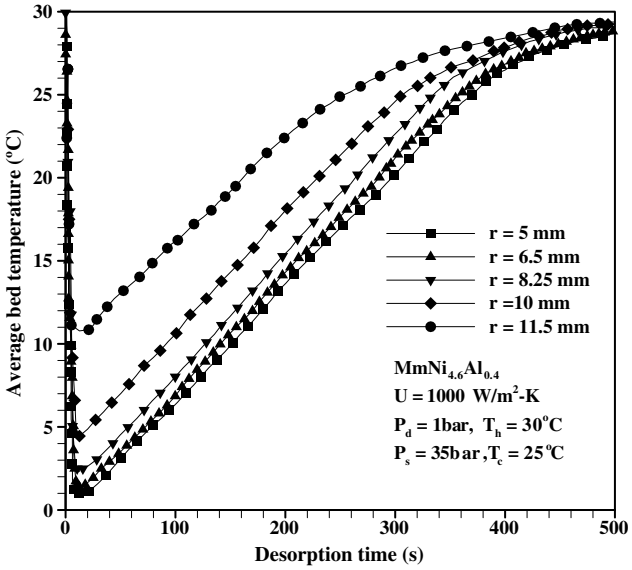


Fig. 7. Variation of average bed temperature at different radial positions for $MmNi_{4.6}Al_{0.4}$.

3.2. Radial variations in bed temperature and hydrogen concentration profiles

It is observed from Figs. 6 and 7 that the temperature of the hydride bed increases continuously from the porous filter to the convective wall in the radial direction. This is due to the effect of heat transfer from the hot fluid flowing around the bed to the hydride bed. The region close to the porous filter experiences less heat transfer compared to that of the convective wall. Due to this behavior, the region close to the porous filter experiences low temperature for long time resulting in poorer dehydriding rate around the porous filter. It is clear from Eq. (2.1) that the bed temperature strongly influences the dehydride equilibrium pressure (P_{eq}). Hence, at high equilibrium pressure, the reaction rate increases due to the higher pressure difference ($P_{eq} - P_d$) in the region close to the convective wall. Figs. 8 and 9 show the variation in the hydride bed concentration along the radial direction and reveal that the rate of hydrogen desorbed in the region close to the convective wall is high due to the rapid absorption of heat from the heat transfer fluid.

3.3. Effect of bed thickness on average bed temperature and hydrogen storage capacity

The thickness of the bed (difference between the outer and inner radii) was varied from 5.0 to 15.0 mm by keeping the inner radius constant at 4.5 mm. Figs. 10 and 11 show the variation of the average bed temperature during desorption of hydrogen. The rate at which the hydrogen desorption in 5.0 mm bed thickness is rapid compared to the other bed thicknesses and also reaches the hot fluid temperature very quickly accompanied by faster heat transfer rate. It is observed from Figs. 12 and 13, for a given bed thickness of 5 mm the desorption of hydrogen is completed quickly within 180 s, while for 10 and 15 mm hydride bed thicknesses it takes

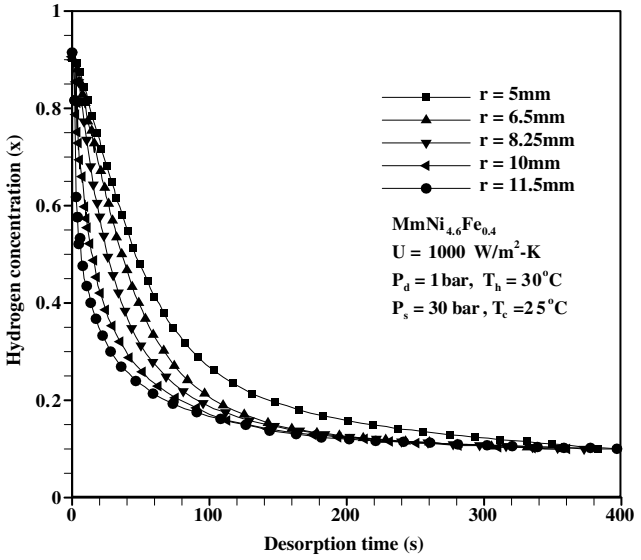


Fig. 8. Variation of hydrogen concentration at different radial positions for $MmNi_{4.6}Fe_{0.4}$.

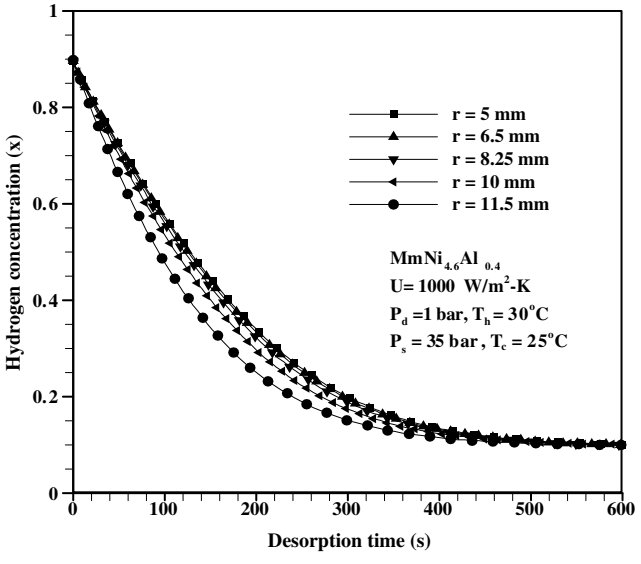


Fig. 9. Variation of hydrogen concentration at different radial positions for $MmNi_{4.6}Al_{0.4}$.

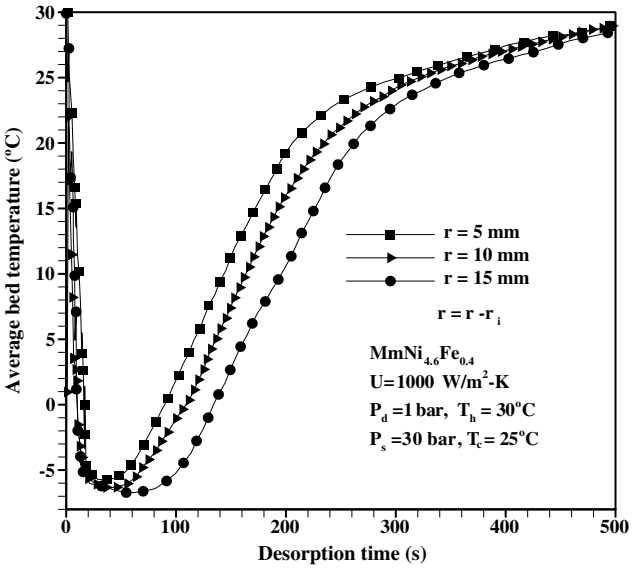


Fig. 10. Effect of bed thickness on average bed temperature for $MmNi_{4.6}Fe_{0.4}$.

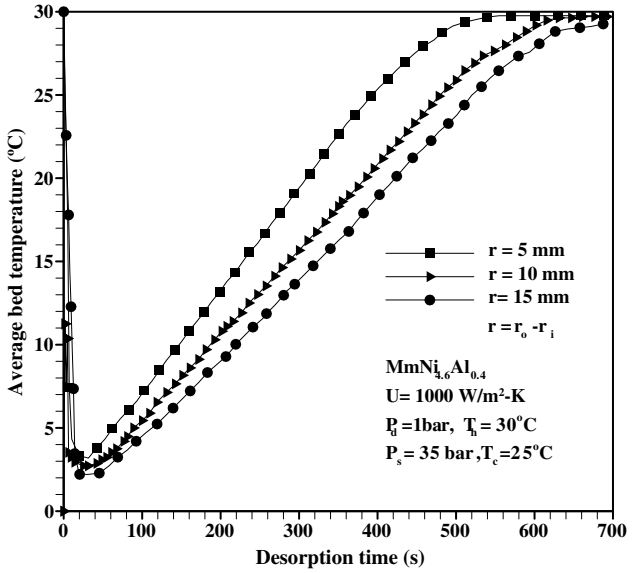


Fig. 11. Effect of bed thickness on average bed temperature for $MmNi_{4.6}Al_{0.4}$.

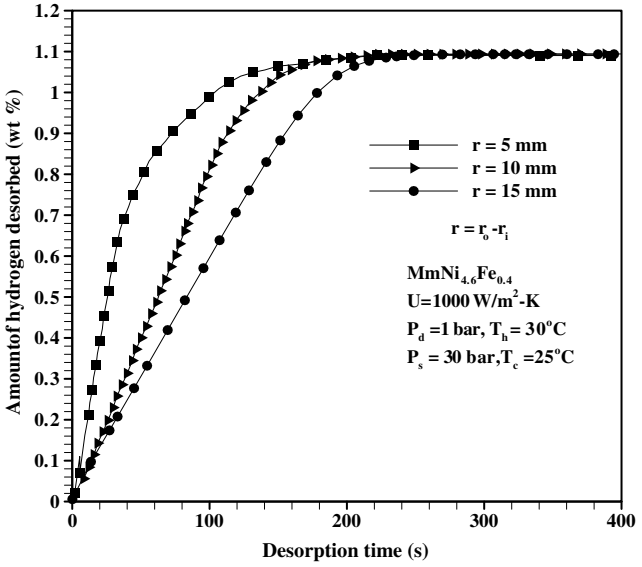


Fig. 12. Effect of bed thickness on amount of hydrogen desorbed for $MmNi_{4.6}Fe_{0.4}$.

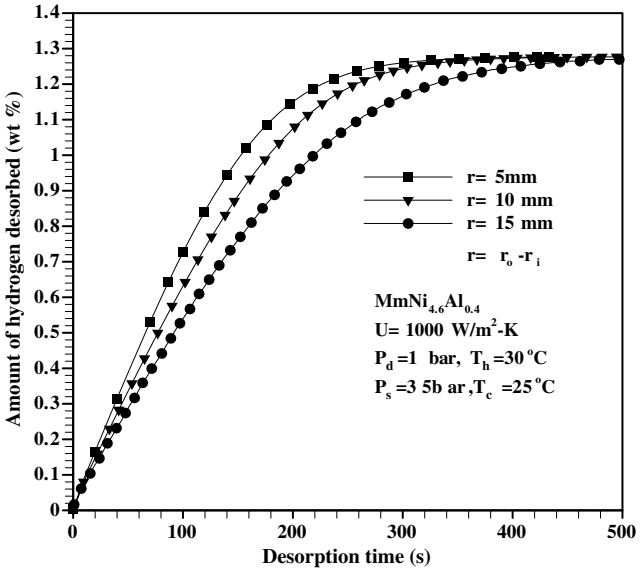


Fig. 13. Effect of bed thickness on amount of hydrogen desorbed for $MmNi_{4.6}Al_{0.4}$.

about 250 and 300 s, respectively, for $MmNi_{4.6}Fe_{0.4}$ alloy. The corresponding desorption times for $MmNi_{4.6}Al_{0.4}$ alloy are 300, 380 and 500 s, respectively, for the bed thicknesses of 5, 10 and 15 mm. It is observed that thin beds are preferred for quicker desorption cycle.

4. Conclusions

A two-dimensional mathematical model to describe the prediction of coupled heat and mass transfer in the hydride bed during desorption of hydrogen has been developed. The computations are performed using the commercial software FLUENT 6.1.22. Desorption characteristics of $MmNi_{4.6}Fe_{0.4}$ and $MmNi_{4.6}Al_{0.4}$ are studied numerically at different hot fluid temperatures varying from 30 to 50 °C and different metal hydride bed thicknesses from 5.0 to 15.0 mm. The numerical results showed good agreement with the experimental data reported in the literature. It is shown that for higher hot fluid temperatures of above 50 °C, desorption time is reduced significantly for both the alloys. At 30 bar supply pressure and 25 °C absorption temperature, $MmNi_{4.6}Fe_{0.4}$ desorbs 1.11 wt% where as $MmNi_{4.6}Al_{0.4}$ desorbs 1.28 wt%. The effect of hydride bed thickness is significant and thin beds are preferred for a quicker desorption cycle.

References

[1] Ram Gopal M, Srinivasa Murthy S. Prediction of heat and mass transfer in annular cylindrical metal hydride beds. Int J Hydrogen Energy 1992;17(10):795–805.
[2] Mayer U, Groll M, Supper W. Heat and mass transfer in metal hydride reaction beds: experimental and theoretical results. J Less-Common Metals 1987;131(1–2):235–44.
[3] Mat D, Kaplan Y. Numerical study of hydrogen absorption in an Lm–Ni_5 hydride reactor. Int J Hydrogen Energy 2001;26(9):957–63.
[4] Jemni A, Ben Nasrallah S. Study of two-dimensional heat and mass transfer during absorption in a metal-hydrogen reactor. Int J Hydrogen Energy 1995;20(1):43–52.
[5] Faouzi Askri, Jemni A, Ben Nasrallah S. Dynamic behavior of metal-hydrogen reactor during hydriding Process. Int J Hydrogen Energy 2004;29(6):635–47.
[6] Nakagawa T, Inomata A, Aoki H, Miura T. Numerical analysis of heat and mass transfer characteristics in the metal hydride bed. Int J Hydrogen Energy 2000;25(4):339–50.
[7] Arvind Kumar Phate, Prakash Maiya M, Srinivasa Murthy S. Simulation of transient heat and mass transfer during hydrogen sorption in cylindrical metal hydride beds. Int J Hydrogen Energy 2007;32(12):1969–81.
[8] Philippe Marty, Fourmigue JF, De Rango P, Fruchart D, Charbonnier J. Numerical simulation of heat and mass transfer during the absorption of hydrogen in a magnesium hydride. Energy Convers Manage 2006;47(20):3632–43.
[9] Ram Gopal M, Srinivasa Murthy S. Parametric studies on heat and mass transfer in metal hydride beds. Chem Eng Process 1993;32(4):217–23.
[10] Jemni A, Ben Nasrallah S. Study of two-dimensional heat and mass transfer during desorption in a metal-hydrogen reactor. Int J Hydrogen Energy 1995;20(11):881–91.
[11] Jemni A, Ben Nasrallah S, Lamloumi J. Experimental and theoretical study of a metal-hydrogen reactor. Int J Hydrogen Energy 1999;24(7):631–44.
[12] Faouzi Askri, Jemni A, Ben Nasrallah S. Prediction of transient heat and mass transfer in a closed metal-hydrogen reactor. Int J Hydrogen Energy 2004;29(2):195–208.
[13] Faouzi Askri, Jemni A, Ben Nasrallah S. Study of two-dimensional and dynamic heat and mass transfer in a metal-hydrogen reactor. Int J Hydrogen Energy 2003;28(5):537–57.
[14] Isselhorst A. Heat and mass transfer in coupled hydride reaction beds. J Alloys Compounds 1995;231(1–2):871–9.
[15] Muthukumar P, Madhavakrishna U, Anupam Dewan. Parametric studies on a metal hydride based hydrogen storage device. Int J Hydrogen Energy 2007;32(18):4988–97.
[16] Muthukumar P, Prakash Maiya M, Srinivasa Murthy S. Experiments on a metal hydride-based hydrogen storage device. Int J Hydrogen Energy 2005;30(15):1569–81.
[17] Patankar SV. Numerical heat transfer and fluid flow. New York: Hemisphere; 1980.